ChemInform Abstract: Electronic Ground States of Low-Spin Iron(III) Porphyrinoids

ARTICLE *in* JOURNAL OF INORGANIC BIOCHEMISTRY · APRIL 2008

Impact Factor: 3.44 · DOI: 10.1016/j.jinorgbio.2007.10.024 · Source: PubMed

3 AUTHORS, INCLUDING:

Mikio Nakamura
Toho University
177 PUBLICATIONS **2,659** CITATIONS
SEE PROFILE

Yoshiki Ohgo
Teikyo University
106 PUBLICATIONS **1,106** CITATIONS
SEE PROFILE

Available online at www.sciencedirect.com
ScienceDirect
Journal of Inorganic Biochemistry 102 (2008) 433–445
Journal of Inorganic Biochemistry
www.elsevier.com/locate/jinorgbio

Electronic ground states of low-spin iron(III) porphyrinoids

Mikio Nakamura [a,b,c,*], Yoshiki Ohgo [a,b], Akira Ikezaki [a]

[a] Department of Chemistry, Faculty of Medicine, Toho University, Ota-ku, Tokyo 143-8540, Japan
[b] Research Center for Materials with Integrated Properties, Toho University, Funabashi 274-8510, Japan
[c] Division of Chemistry, Graduate School of Science, Toho University, Funabashi 274-8510, Japan

Received 8 July 2007; received in revised form 29 September 2007; accepted 12 October 2007
Available online 24 November 2007

Abstract

Six-coordinate low-spin iron(III) porphyrinates adopt either common $(d_{xy})^2(d_{xz},d_{yz})^3$ or less common $(d_{xz},d_{yz})^4(d_{xy})^1$ ground state. In this review article, three major factors that affect the electronic ground state have been examined. They are (i) nature of the axial ligand, (ii) electronic effect of peripheral substituents, and (iii) deformation of porphyrin ring. On the basis of the ^{1}H NMR, ^{13}C NMR, and EPR data, it is now clear that (i) the axial ligands with low-lying π^* orbitals such as *tert*-butylisocyanide and 4-cyanopyridine, (ii) the electron donating groups at the *meso*-carbon atoms, and (iii) the ruffled deformation of porphyrin ring stabilize the $(d_{xz},d_{yz})^4(d_{xy})^1$ ground state. By manipulating these factors, we are able to prepare various low-spin iron(III) porphyrinates with unusual electronic structures such as bis(imidazole) complexes with the $(d_{xz},d_{yz})^4(d_{xy})^1$ ground state or bis(*tert*-butylisocyanide) complexes with the $(d_{xy})^2(d_{xz},d_{yz})^3$ ground state; bis(imidazole) and bis(*tert*-butylisocyanide) complexes usually adopt the $(d_{xy})^2(d_{xz},d_{yz})^3$ and $(d_{xz},d_{yz})^4(d_{xy})^1$ ground state, respectively.

Keywords: Iron(III) porphyrinoids; Low-spin complexes; Electronic ground state axial ligands; Electronic effects of peripheral substituents; Deformation of porphyrin ring; NMR spectroscopy; EPR spectroscopy

1. Introduction

Heme proteins are playing fundamental roles in biological systems such as oxygen transport in hemoglobin, oxygen storage in myoglobin, electron transfer in various cytochromes, and oxidation of organic substrates in cytochrome P450 [1]. These phenomena are closely connected with the electronic structure of heme, i.e. an iron porphyrinate, located in the active site of heme proteins. Typical examples are the reactions catalyzed by cytochrome P450 as shown in Fig. 1 [2]. In the resting state (A) of cytochrome P450, iron adopts six-coordinate ferric low-spin state, $S = 1/2 Fe^{III}$–OH_2, with cysteinate and water as axial ligands. However, once organic substrate is incorporated into the substrate binding pocket, all the water molecules in the pocket are excluded and consequently the iron adopts five-coordinate ferric high-spin state (B), $S = 5/2$ Fe^{III}, with cysteinate as the sole axial ligand. The redox potential increases on going from the $S = 1/2$ Fe^{III}–OH_2 to the $S = 5/2$ Fe^{III} state, which makes the reduction of the iron much easier and leads to the formation of five-coordinate ferrous high-spin state (C), $S = 2$ Fe^{II}, having a single cysteinate axial ligand. Following is the oxygen binding step as in the case of hemoglobin and myoglobin. Addition of dioxygen to the $S = 2$ Fe^{II} forms oxygen-bound diamagnetic species which is expressed either as six-coordinate ferrous low-spin, $S = 0$ Fe^{II}–O_2, or six-coordinate ferric low-spin superoxo species (D), Fe^{III}–$O_2^{\cdot}$. A very labile low-spin ferric peroxo species (E), Fe^{III}–O_2^-, is then formed by a second one-electron reduction. This complex receives two protons and releases one water molecule to form reactive intermediate which is believed to be six-coordinate low-spin ferryl-oxo species with radical cationic porphyrin (F), $P^{\cdot+}$–Fe^{IV}=O [3].

* Corresponding author. Address: Department of Chemistry, Faculty of Medicine, Toho University, Ota-ku, Tokyo 143-8540, Japan. Tel.: +81 457 822 606; fax: +81 3 5493 5430.
E-mail address: mnakamu@med.toho-u.ac.jp (M. Nakamura).

0162-0134/$ - see front matter © 2007 Elsevier Inc. All rights reserved.
doi:10.1016/j.jinorgbio.2007.10.024

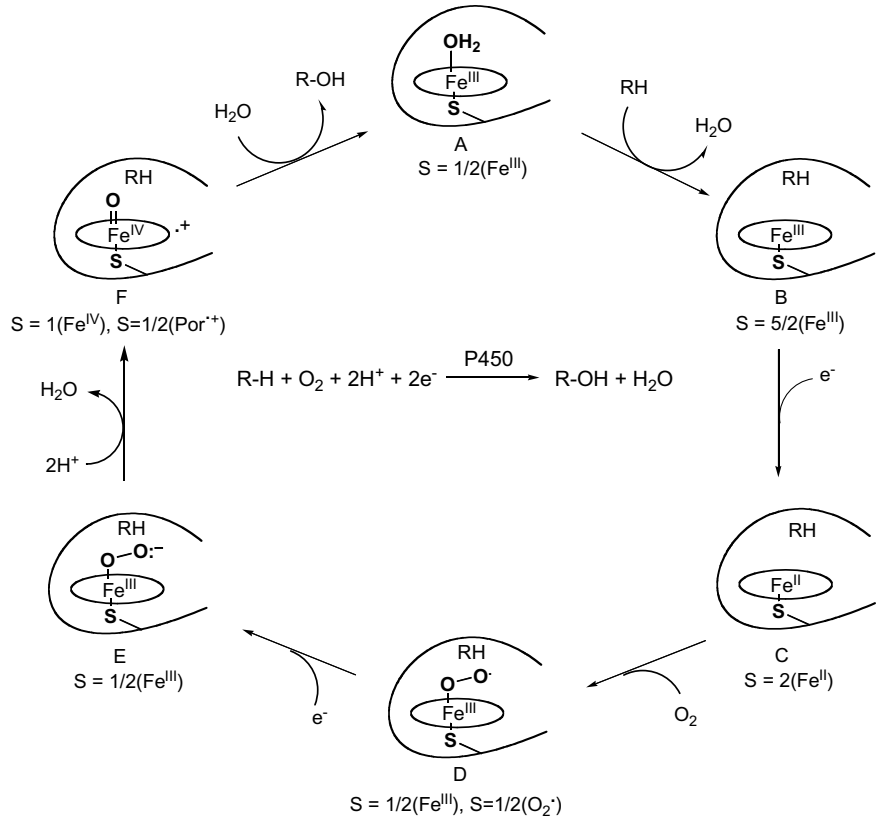

Fig. 1. Changes in electronic structures of iron porphyrinates during the catalytic cycle in cytochrome P450.

As this example shows explicitly, the iron porphyrinate changes its electronic structure in each step of the catalytic cycle. Thus, it is very important to reveal the detailed physicochemical properties of the complexes with various electronic structures. The use of model complexes is quite suitable for this purpose because we can characterize them by means of a number of techniques such as NMR, EPR, resonance Raman, MCD, Mössbauer, EXAFS, SQUID, and X-ray crystallography [4,5]. In addition these measurements can be done even at extreme conditions that are sometimes difficult to perform in proteins. Furthermore, by manipulating the d orbital energy levels, we are able to obtain various complexes with novel electronic structures. The new results obtained from the model study should be helpful for deeper understanding of the biological reactions.

In iron(III) porphyrinates, there are three kinds of spin states; high-spin ($S = 5/2$), low-spin ($S = 1/2$), and intermediate-spin ($S = 3/2$) state. Through the extensive studies using model complexes, it is now clear that the spin states are controlled by various factors [6]. While the six-coordinate complexes carrying axial ligands with strong field strength such as HIm and CN^- always exhibit a low-spin ($S = 1/2$) state, those with weak oxygen ligands such as pyridine N-oxide, DMSO, methanol, and THF show the spin state which changes from a nearly pure high-spin to a nearly pure intermediate-spin state [7]. In this short review article, we would like to focus our attention on the electronic structures of six-coordinate low-spin iron(III) porphyrinates because this spin state is most frequently seen in naturally occurring heme proteins. In addition, special emphasis has been placed on extracting the factors that affect the electronic ground states of low-spin iron(III) porphyrinates.

2. Spectroscopic methods to determine the electronic ground states

Recent extensive studies have revealed that six-coordinate low-spin iron(III) porphyrinates adopt either the common $(d_{xy})^2(d_{xz}, d_{yz})^3$or the less common $(d_{xz}, d_{yz})^4(d_{xy})^1$ ground state as shown in Fig. 2 depending on the various factors [7–10]. In many cases, complexes carrying axial ligands with strong σ-donating ability such as HIm and CN^- adopt the common $(d_{xy})^2(d_{xz}, d_{yz})^3$ ground state. In

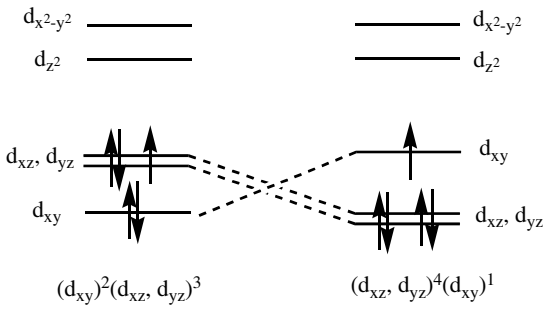

Fig. 2. Electron configuration of low-spin iron(III) porphyrin complexes.

these complexes, the unpaired electron in one of the d_π orbitals delocalizes to the porphyrin ring especially on the pyrrole β-carbon atoms through the interaction with the porphyrin $3e_g$ orbital shown in Fig. 3; the $3e_g$ orbital has relatively large coefficients at the nitrogen and pyrrole β-carbon atoms and zero coefficient at the *meso* carbon atoms. In contrast, complexes carrying axial ligands with weak σ-donating and strong π-accepting ability such as ^{t}BuNC and 4-CNPy prefer the less common $(d_{xz}, d_{yz})^4(d_{xy})^1$ ground state. Walker, Scheidt and others explained the formation of the less common $(d_{xz}, d_{yz})^4(d_{xy})^1$ type complexes in terms of the interaction between iron d_π and ligand p^*_π orbital [11–13]. Because of this interaction, the iron d_π orbitals are stabilized to the points, which are lower than the d_{xy} orbital. As a result, the unpaired electron occupies the d_{xy} orbital to form the $(d_{xz}, d_{yz})^4(d_{xy})^1$ ground state. Furthermore, the d_{xy} orbital is destabilized if the porphyrin ring is ruffled because the ruffling makes the interaction between the half-filled iron d_{xy} and filled porphyrin a_{2u} orbital shown in Fig. 3 possible; both the d_{xy} and a_{2u} orbitals in D_{4h} complexes are represented as b_2 in ruffled D_{2d} complexes [14,15]. In fact, the X-ray crystallographic data have

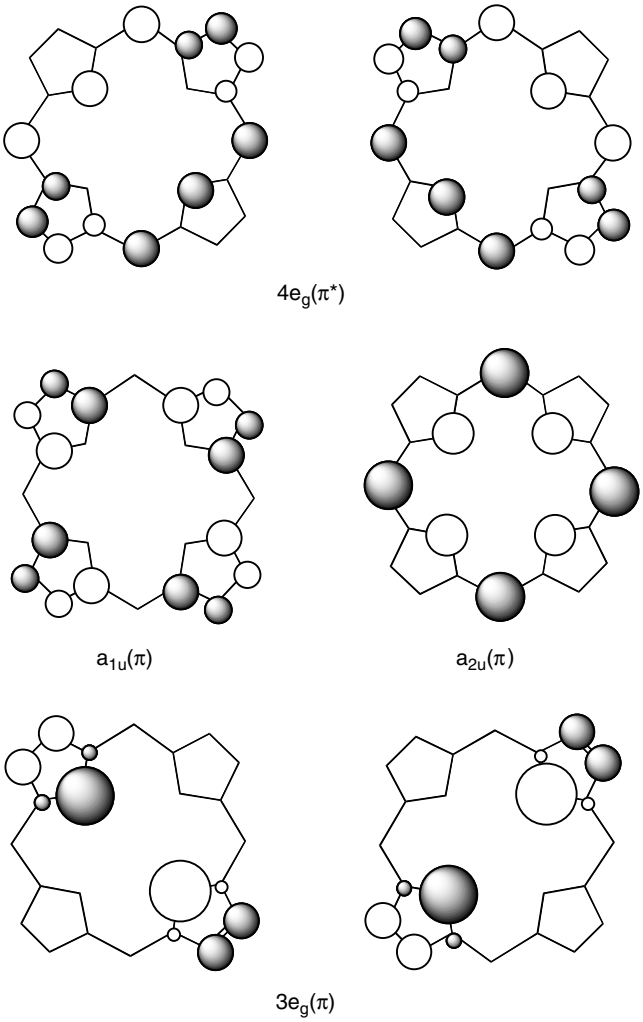

Fig. 3. Frontier orbitals of porphyrin.

revealed that almost all the low-spin complexes adopting the $(d_{xz}, d_{yz})^4(d_{xy})^1$ ground state have exhibited the ruffled porphyrin core [12,16–18]. The d_{xy}–a_{2u} interaction in ruffled complexes induces a sizable amount of spin densities on the *meso* carbon atoms since the a_{2u} orbital has large coefficient on these atoms. Depending on the energy difference between the d_{xy} and d_π orbitals, thermally accessible excited states with different electron configurations such as $(d_{xz}, d_{yz})^3(d_{xy})^2$ contribute to the electronic ground state of the complex. If the d_{xy} orbital is located far above the d_π orbitals in energy diagram, then the complex has a quite pure $(d_{xz}, d_{yz})^4(d_{xy})^1$ ground state. If, on the other hand, the energy difference is rather small, then the contribution of the excited state increases.

Electronic ground states can be determined by the ^{1}H and ^{13}C NMR spectra [7–10,19–23]. As mentioned, the $(d_{xy})^2(d_{xz}, d_{yz})^3$ type complexes are expected to have relatively large spin density on the β-pyrrole carbon and zero spin density on the *meso* carbon atoms. Thus, the pyrrole-H and *meso*-C signals shift to the upfield position relative to those of the corresponding diamagnetic complex. Typical example is $[Fe(TPP)(HIm)_2]^+$ where the pyrrole-H and *meso*-C signals appear at −16.6 and 55 ppm, respectively, in CD_2Cl_2 at 298 K [24,25]. By contrast, the $(d_{xz}, d_{yz})^4(d_{xy})^1$ type complexes exhibit the pyrrole-H signal close to the diamagnetic position and *meso*-C signal at an extremely downfield position. Typical example is $[Fe(TPP)(^t BuNC)_2]^+$ where the pyrrole-H and *meso*-C appear at 9.73 and 767 ppm, respectively [25–27]. Presence of an extremely downfield shifted *meso*-C signal indicates that the *meso*-carbons actually have fairly large amounts of spin density due to the interaction between half-filled d_{xy} and filled a_{2u} orbital in ruffled $[Fe(TPP)(^t BuNC)_2]^+$ [25]. These results indicate that the pyrrole-H and *meso*-C signals in low-spin $[Fe(TPP)L_2]^+$ appear in the range −18 to +10 ppm and 55–770 ppm, respectively, at ambient temperature depending on the electronic ground state. Thus, these two signals can be good probes to reveal the electronic ground state of low-spin complexes. It should be noted, however, that the chemical shift ranges of the pyrrole-H and *meso*-C signals mentioned above are applicable only to the low-spin complexes signified by $[Fe(TPP)L_2]^+$; the chemical shift ranges are different in other types of low-spin complexes such as $[Fe(TRP)L_2]^{\pm}$ and $[Fe(OETPP)L_2]^{\pm}$ which have intrinsically ruffled and saddled porphyrin core, respectively.

Another convenient method to probe the electronic ground state of low-spin iron(III) porphyrinates such as $[Fe(TPP)L_2]^+$ and $[Fe(TPC)L_2]^+$ is to calculate the $\delta_m - \delta_p$ and $\delta_m - \delta_o$ values; δ_o, δ_m, and δ_p are the chemical shifts of the *o*-, *m*-, and *p*-phenyl signals, respectively [9]. If $\delta_m - \delta_p$ and $\delta_m - \delta_o$ are both large and positive, then the complex has large amounts of positive spin at the *meso*-carbons, which in turn indicate that the complex adopts the $(d_{xz}, d_{yz})^4(d_{xy})^1$ ground state. In contrast, if $\delta_m - \delta_p$ and $\delta_m - \delta_o$ are small with $\delta_m - \delta_p$ positive and $\delta_m - \delta_o$ usually negative, then the complex adopts the $(d_{xy})^2(d_{xz}, d_{yz})^3$

ground state since the *meso*-carbons have little or no spin density.

Electronic ground state of low-spin complexes can most clearly be determined by EPR spectroscopy that is usually taken at extremely low temperatures [7–10,28,29]. Complexes with the common $(d_{xy})^2(d_{xz},d_{yz})^3$ ground state exhibit either rhombic or large g_{max} type spectra as shown in Fig. 4a and b, respectively, depending upon the orientation of axial ligands [8–10,25,30]. If planar axial ligands such as imidazole and pyridine take mutually parallel alignment above and below the porphyrin ring, the complexes exhibit the rhombic type spectra. If, on the contrary, they take mutually perpendicular alignment, the complexes exhibit single-feature large g_{max} type spectra where a strong signal is observed above $g = 3.2$ [10]. EPR spectra shown in Fig. 4a and b, are those of $[Fe(OEP)(DMAP)_2]^+$ and $[Fe(OETPP)(DMAP)_2]^+$, respectively, taken in CH_2Cl_2 solutions at 4.2 K [30]. Complexes with linear ligands such as cyanide also exhibit the large g_{max} type spectra. In contrast, the $(d_{xz},d_{yz})^4(d_{xy})^1$ type complexes carrying axial ligands with low-lying π^* orbitals adopt the axial type spectra with $-g_x = g_y > 0$ and $g_z < 0$ as in the case of $[Fe(T^nPrP)(4\text{-}CNPy)_2]^+$ shown in Fig. 4c [25]. Once the EPR g values are obtained, it is possible to estimate the energy gap between the d_{xy} and d_π orbitals [28,31,32].

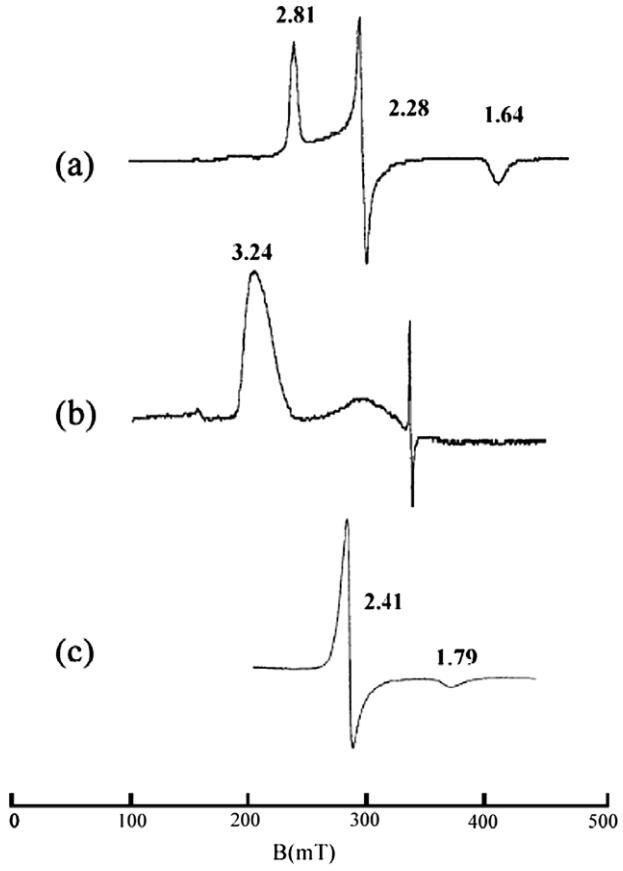

Fig. 4. EPR spectra of (a) $[Fe(OEP)(DMAP)_2]^+$, (b) $[Fe(OETPP)(DMAP)_2]^+$, and (c) $[Fe(T^nPrP)(4\text{-}CNPy)_2]^+$ taken in frozen CH_2Cl_2 solutions at 4.2 K; typical examples showing the large g_{max}, rhombic, and axial type spectra, respectively. Adapted from Ref. [30,36].

3. Factors affecting the electronic ground states

There are several factors that affect the electronic ground states of low-spin iron(III) porphyrinates. Three major factors that should be considered are (i) number and nature of axial ligands, (ii) electronic effects of peripheral substituents, and (iii) deformation of porphyrin rings. Among these factors, the number and nature of the axial ligands are the most important factor that affects the electronic ground state of low-spin iron(III) porphyrinates. In this section, we will describe in detail how these factors affect the electronic ground state of low-spin complexes by using various model complexes given in Scheme 1.

3.1. Axial ligands

Axial ligands with strong σ and π donating ability such as HIm and DMAP adopt the common $(d_{xy})^2(d_{xz},d_{yz})^3$ ground state, while those with low-lying π^* orbitals such as 4-CNPy and ^{t}BuNC prefer the less common $(d_{xz},d_{yz})^4(d_{xy})^1$ ground state. Safo and co-workers have measured the ^{1}H NMR chemical shifts of $[Fe(TMP)L_2]^+$ shown in Scheme 1a and have correlated them with the $pK_a(BH^+)$ values of a wide variety of nitrogen bases (L's) ranging from 9.7 (DMAP) to 1.1 (4-CNPy) [11]. Table 1 lists the chemical shifts (δ_{obs}) and isotropic shifts (δ_{iso}) of *m*-H and pyrrole-H signals together with the pK_a values of the conjugate acids; the isotropic shift is defined by $\delta_{iso} = \delta_{obs} - \delta_{dia}$, where δ_{dia} is the chemical shift of the corresponding signal in analogous diamagnetic complexes. The data in Table 1 indicate that the isotropic shift of *m*-H increases while that of pyrrole-H decreases as the axial ligand becomes less basic. The result is interpreted in terms of a smooth change in electronic ground state from a largely $(d_{xy})^2(d_{xz},d_{yz})^3$ to at least 50% $(d_{xz},d_{yz})^4(d_{xy})^1$ as the energy level of the ligand π^* orbital decreases.

Simonneaux and co-workers have reported that iron(III) porphyrinates with phosphonite derivatives such as $P(OMe)_2Ph$ and $P(OEt)_2Ph$ also exhibit the $(d_{xz},d_{yz})^4(d_{xy})^1$ ground state as revealed from the ^{1}H NMR and EPR data [33]. The pyrrole-H signal appears at +2.6 ppm at 293 K for $[Fe(TPP)(P(OEt)_2Ph)]^+$ shown in Scheme 1b where X = H and L = $P(OEt)_2Ph$. The EPR spectrum is axial with $g_\perp = 2.36$ and $g_\parallel = 1.91$ for $[Fe(T(p\text{-}Me)PP)(P(OEt)_2Ph)]^+$ [17]. In contrast, the corresponding bis(phosphine) complex $[Fe(TPP)(PMe_3)_2]^+$ adopts the $(d_{xy})^2(d_{xz},d_{yz})^3$ ground state as revealed from the upfield shifted pyrrole-H signal, i.e. −19.6 ppm at 303 K [34]. Since the pK_a values of the conjugate acids of phosphorous ligands decrease in the order $PMe_3 > PMe_2Ph > P(OMe)_2Ph > P(OMe)_3$[35], the result can be ascribed to the presence of the low-lying π^* orbital in phosphonite ligands. The $\delta_m - \delta_p$ and $\delta_m - \delta_o$ values for $[Fe(TPP)(PPh(OEt)_2)]^+$ are 6.34 and 4.64 ppm, respectively, while those for $[Fe(TPP)(PMe_3)_2]^+$ are 0.42 and 1.78 ppm, respectively, supporting for the above-mentioned assignment of the ground state [9].

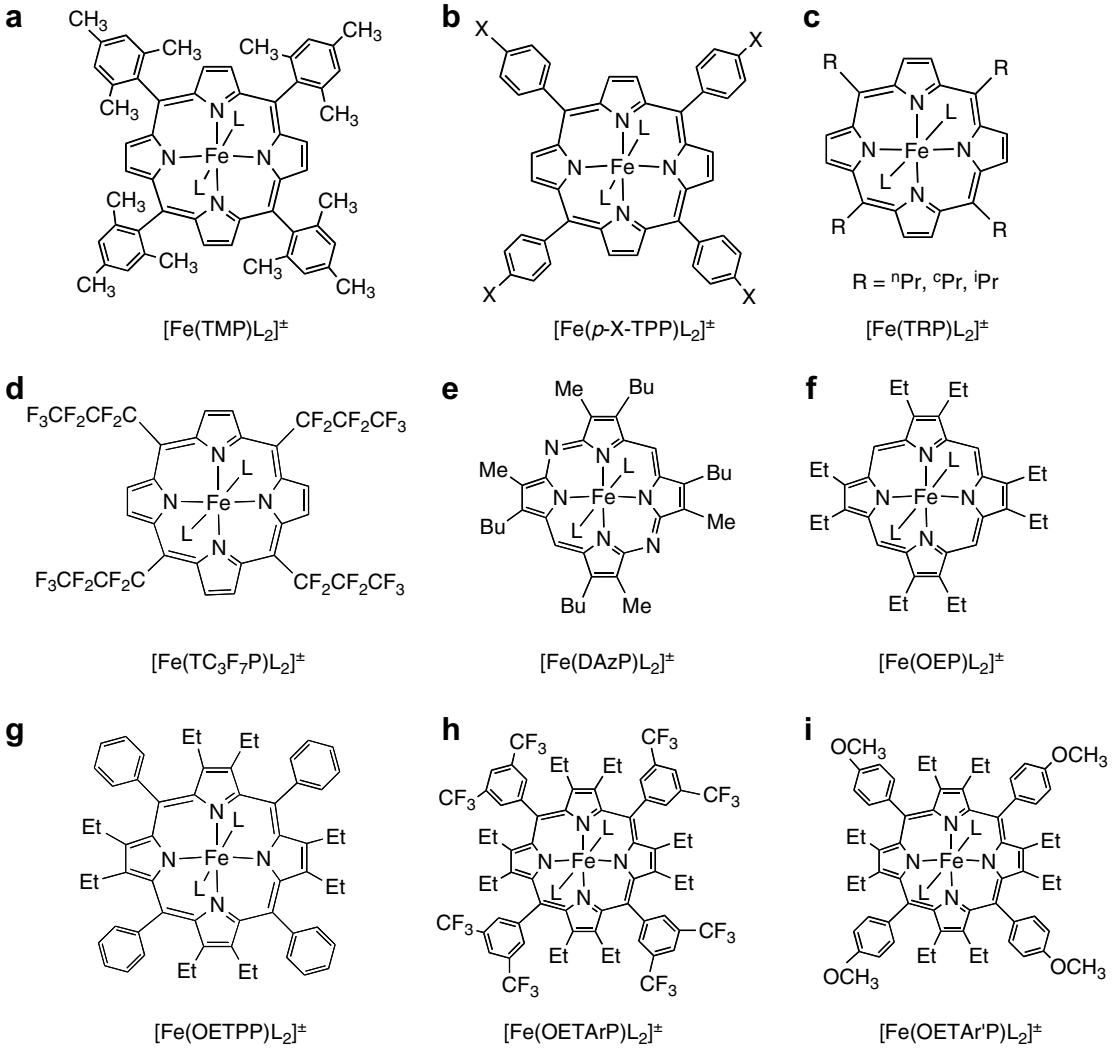

Scheme 1. Various low-spin complexes: (a) $[Fe(TMP)L_2]^{\pm}$, (b) $[Fe(TRP)L_2]^{\pm}$, (c) $[Fe(T(p\text{-}X)PP)L_2]^{\pm}$, (d) $[Fe(T(C_3F_7)P)L_2]^{+}$, (e) $[Fe(DAzP)L_2]^{+}$, (f) $[Fe(OEP)L_2]^{+}$, (g) $[Fe(OETPP)L_2]^{\pm}$, (h) $[Fe(OETArP)L_2]^{\pm}$, and (i) $[Fe(OETAr'P)L_2]^{\pm}$. Ar and Ar′ in (h) and (i) are 3,5-bis(trifluoromethyl)phenyl and 4-methoxyphenyl group, respectively.

Table 1
^{1}H NMR chemcial shifts of a series of $[Fe(TMP)L_2]^+$at 193 K in CD_2Cl_2

Ligand	pK_a (BH^+)	δ_{obs}		δ_{iso}	
		m-H	Py-H	m-H	Py-H
DMAP	9.70	4.85	−30.9	−2.42	−39.5
2-Melm	7.56	7.77	−20.4	+0.5	−29.0
1-Melm	7.33	5.01	−31.3	−2.26	−39.9
3,4-Me_2Py	6.46	7.48	−21.2	+0.21	−29.7
3,5-Me_2Py	6.15	7.12	−23.0	−0.15	−31.6
4-MePy	6.02	8.22	−18.2	+0.95	−26.8
3-MePy	5.68	8.36	−17.8	+1.09	−26.4
Py	5.22	9.47	−13.3	+2.20	−21.9
3-CIPy	2.84	10.85	−10.3	+3.58	−18.9
3-CNPy	1.45	13.07	−4.4	+5.80	−13.0
4-CNPy	1.1	14.59	+2.1	+7.32	−6.5

Adapted from Ref. [11].

Change in electronic ground state is more explicitly seen if phenyl groups at the *meso* positions are replaced by alkyl groups. Table 2 lists the ^{1}H and ^{13}C NMR chemical shifts (CD_2Cl_2, 223 K) of a series of $[Fe(T^nPrP)L_2]^{\pm}$ shown in Scheme 1c, where R = ^{n}Pr [25,36]. The EPR *g* values (CH_2Cl_2, 4.2 K) are also listed. The ligands are arranged in the ascending order of the pyrrole-H chemical shifts except for 4-CNPy and ^{t}BuNC; the pyrrole-H chemical shift of the bis(4-CNPy) complex is slightly larger than that of the bis(^{t}BuNC) complex. This order corresponds to the ascending order of the *meso*-CH and *meso*-C chemical shifts. The large downfield shifts of the pyrrole-H and *meso*-C signals, which is observed when the axial ligand changes from HIm to ^{t}BuNC, are indicative of a smooth shift of the electronic ground state from nearly pure $(d_{xy})^2(d_{xz},d_{yz})^3$ to nearly pure $(d_{xz},d_{yz})^4(d_{xy})^1$. The EPR data are also consistent with the NMR data in a sense that the three complexes from the top show the rhombic type spectra while the other four complexes exhibit the axial type spectra. Furthermore, the $g_{\perp}$ value approaches to 2.0 on going from CN^- to ^{t}BuNC though a small reversal is observed between CN^- and Py. The energy gaps between

Table 2
^{1}H and ^{13}C NMR chemical shifts(CD_2Cl_2, 223 K) and EPR g values (CH_2Cl_2, 4.2 K) of $[Fe(T^nPrP)L_2]^{\pm}$

L	^{1}H NMR		^{13}C NMR	EPR			Electron configuration[a]
	Py-H	*meso*-CH	*meso*-C	g_1	g_2	g_3	
HIm	−21.5	1.7	73.1	2.90	2.35	1.45[b]	dπ
DMAP	−16.7	9.7	130.5	3.10	2.10	–	dπ
2-MeIm	−8.2	21.3	n.d.	2.85	2.10	–	dπ
CIST	−3.5	30.9	336.1	2.51	2.51	–	d_{xy}
Py	7.1	57.9	526.5	2.55	2.55	–	d_{xy}
4-CNPy	13.0	88.5	814.7	2.46	2.46	1.68	d_{xy}
^{t}BuNC	12.7	118.5	[c]	2.16	2.16	1.95	d_{xy}

Adapted from Refs. [25,36].
[a] Determined on the basis of the EPR g values.
[b] Calculated value.
[c] Not observed.

the d_{xy} and d_π orbitals for $[Fe(T^nPrP)(4\text{-}CNPy)_2]^+$ and $[Fe(T^nPrP)(^tBuNC)_2]^+$ are calculated to be 3.5λ and 10.7λ, respectively, from the EPR g values, where λ is the spin–orbit coupling constant. We can therefore conclude that the contribution of the $(d_{xz}, d_{yz})^4(d_{xy})^1$ ground state increases as the axial ligand changes from HIm to ^{t}BuNC according to the order given below:

$$\text{HIm, 1-MeIm, DMAP} < \text{2-MeIm} < CN^- < \text{Py} < \text{3-CNPy, 4-CNPy} < {}^t\text{BuNC}$$

3.2. Electronic effects of peripheral substituents

In addition to the field strengths of axial ligands, electronic ground state can also be affected by the electronic effect of peripheral substituents. Table 3 lists the ^{1}H and ^{13}C NMR chemical shifts of a series of $[Fe(T(p\text{-}X)PP)(CN)_2]^-$ shown in Scheme 1b [37]. Fig. 5 shows the Hammett plots for the (a) pyrrole-H and (b) *meso*-C isotropic shifts, where the isotropic shifts determined in CD_2Cl_2 and CD_3OD solutions are plotted against Hammett σ_p values of *p*-X substituents in a series of $[Fe(T(p\text{-}X)PP)(CN)_2]^-$. As shown in Fig. 5a, the pyrrole-H isotropic shifts are by 6–10 ppm much smaller in CD_3OD than those in CD_2Cl_2 solution. By contrast, the *meso*-C isotropic shifts shown in Fig. 5b are by 60–120 ppm much larger in CD_3OD than those in CD_2Cl_2. The results indicate that the spin population in the d_π orbital decreases while that in the d_{xy} orbital increases in each complex as the solvent changes from CD_2Cl_2 to CD_3OD. The spectral change can best be interpreted in terms of the hydrogen bonding between CD_3OD and cyanide [37–44]; the hydrogen bonding lowers the energy level of the cyanide p^*_π orbital and consequently increases the $(d_{xz}, d_{yz})^4(d_{xy})^1$ ground state. Importantly, the negative slopes in Hammett plots are much larger in CD_3OD solutions than in CD_2Cl_2 solutions, which indicate that the electron donating groups at the *meso* positions stabilize the $(d_{xz}, d_{yz})^4(d_{xy})^1$ ground state while the electron withdrawing groups stabilize the $(d_{xy})^2(d_{xz}, d_{yz})^3$ ground state.

There is another good example showing that the electron withdrawing *meso* substituents stabilize the $(d_{xy})^2(d_{xz}, d_{yz})^3$ ground state. Let us compare the spectroscopic data of $[Fe(TPP)(^tBuNC)_2]^+$ with those of $[Fe(F_{20}\text{-}TPP)(^tBuNC)_2]^+$. Porphyrin ring in the latter complex should be electron deficient because of the presence of strongly electron withdrawing pentafluorophenyl (C_6F_5) groups at the *meso* positions. In accordance with the general tendency that bis(^{t}BuNC) complexes adopt the less common $(d_{xz}, d_{yz})^4(d_{xy})^1$ ground state, both of these complexes exhibit the axial type EPR spectra. However, the $g_\perp$ values are quite different; the former is 2.18 while the latter is 2.31 [25]. The result clearly indicates that the d_{xy} orbitals of both complexes are located above the d_π orbitals, but that the energy gap between the d_{xy} and d_π orbital in $[Fe(TPP)(^tBuNC)_2]^+$ is much larger than that in $[Fe(F_{20}\text{-}TPP)(^tBuNC)_2]^+$. Hence, the electron withdrawing *meso* substituents stabilize the $(d_{xy})^2(d_{xz}, d_{yz})^3$ ground state.

Table 3
NMR chemical shifts of $[Fe(p\text{-}X\text{-}TPP)(CN)_2]^-$ determined in CD_2Cl_2 and CD_3OD at 298 K: (a) ^{1}H NMR and (b)^{13}C NMR

X	CD_2CI_2			CD_3OD		
	Py	*o*	*M*	Py	*o*	*m*
(a) ^{1}H NMR chemical shifts						
–OCH_3	−16.09	4.48	5.97	−6.31	5.47	7.80
–CH_3	−16.12	4.47	6.26	−6.78	5.46	8.06
–H	−16.55	4.55	6.36	−7.69	5.61	8.04
–F	−16.82	4.50	6.00	−8.32	5.65	7.62
–Cl	−16.97	4.44	6.27	−8.98	5.57	7.82
–CF_3	−17.62	4.56	6.45	−10.46	5.73	7.86
–CN	−17.62	4.51	6.46	−11.11	5.66	7.80

X	CD_2CI_2				CD_3OD			
	meso	α	β	ipso	*meso*	α	β	ipso
(b) ^{13}C NMR chemical shifts								
–OCH3	94.4	40.2	89.8	118.0	203.9	21	88.3	89.5
–CH_3	93.5	40.3	89.9	123.1	195.8	22.4	88.6	96.6
–H	89.0	41.3	90.3	127.2	183.8	26.6	89.4	103.8
–F	84.2	42.4	90.6	124.1	173.2	30.7	90.2	102.7
–Cl	81.1	42.9	90.9	127.3	163.7	33.3	90.8	107.9
–CF_3	74.8	43.9	91.6	134.1	145.8	38.5	92.4	119.0
–CN	74.3	47.3	92.9	135.8	136.5	41.3	93.3	122.5

Adapted from Ref. [37].

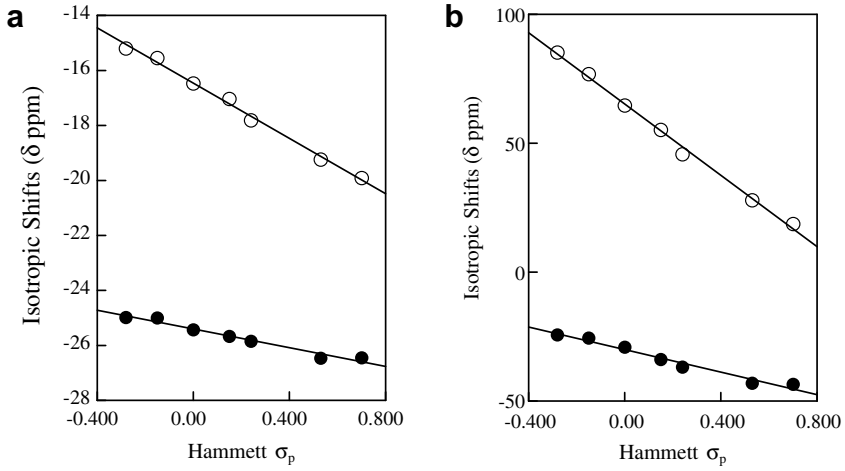

Fig. 5. Hammett plots for the isotropic shifts of the (a) pyrrole-H and (b) *meso*-C in a series of $[Fe(T(p\text{-}X)PP)(CN)_2]^-$. Open and filled circles indicate the isotropic shifts determined in CD_3OD and CD_2Cl_2 solutions, respectively. Adapted from Ref. [37].

Electronic effects of peripheral substituents on the electronic ground state can be explained as follows. Electron donating *meso*-substituents should destabilize the porphyrin π orbitals especially the a_{2u} orbital because the a_{2u} orbital has large coefficients at the *meso* positions. As a result, the interaction between the d_{xy} and a_{2u} orbital is strengthened since the energy gap separating these two orbitals decreases as shown in Fig. 6a. In contrast, the electron withdrawing *meso*-substituents stabilize the a_{2u} orbital, and weaken the a_{2u}–d_{xy} interaction as shown in Fig. 6b. Consequently, the energy level of the d_{xy} orbital is lowered and thus the $(d_{xy})^2(d_{xz},d_{yz})^3$ ground state is stabilized. It should be noted here that the low-spin complex with the purest $(d_{xz},d_{yz})^4(d_{xy})^1$ ground state ever reported in literatures is not the bis(^{t}BuNC) complex but the bis(Py) complex with strongly electron withdrawing heptafluoropropyl (C_3F_7) groups at the *meso* positions; $[Fe(T(C_3F_7)P)(Py)_2]^+$ as shown in Scheme 1d where L = Py [45]. This complex shows the $g_\perp$ and $g_\parallel$ signals at 2.07 and 1.99, respectively. The energy gap (Δ) between the d_{xy} and d_π orbitals reaches as much as -26.4λ which is much larger than those of $[Fe(T^nPrP)(Py)_2]^+$ ($g_\perp = 2.55$) and even $[Fe(T^iPrP)(^t BuNC)_2]^+$ ($g_\perp = 2.16$, $g_\parallel = 1.96$; $\Delta/\lambda = -11.3$). At present, it is difficult to explain why this complex adopts the purest $(d_{xz},d_{yz})^4(d_{xy})^1$ ground state despite the presence of strongly electron withdrawing C_3F_7 groups at the *meso* positions. Highly ruffled structure expected for this complex could strengthen the d_{xy}–a_{2u} interaction. Low-lying $4e_g^*$ orbitals of $T(C_3F_7)P$ could stabilize the iron d_π orbitals by the d_π–$4e_g^*$ interactions. Anyway, $[Fe(T(C_3F_7)P)(Py)_2]^+$ should be an ideal complex to reveal the nature of the d_{xy}–a_{2u} interaction together with the spin distribution on the porphyrin ring. Unfortunately, however, this complex is so unstable that the only spectroscopic data reported is the EPR spectrum at 4.2 K [45].

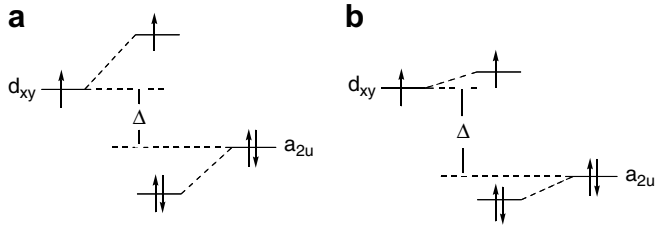

Fig. 6. Schematic representation of the interaction between the d_{xy} and a_{2u} orbitals in low-spin ruffled complexes. Presence of (a) electron donating and (b) electron withdrawing groups at the *meso*-carbons.

3.3. Deformation of porphyrin ring

Table 4a shows the chemical shifts of the pyrrole-H and *meso*-C signals of a wide variety of $[Fe(porphyrin)(L)_2]^{\pm}$, where axial ligands are HIm, CN^-, and ^{t}BuNC [25]. The porphyrins are arranged in the ascending order of the *meso*-C chemical shifts, which also corresponds to the

Table 4
NMR and EPR data of a wide variety of low-spin $[Fe(Porphyrin)L_2]^{\pm}$complexes: (a) ^1H and ^{13}C NMR chemical shifts and (b) EPR *g* values

Porphyrins	L = Him		L = CN^-		L = ^{t}BuNC	
	Py-H	*meso*-C	Py-H	*meso*-C	Py-H	*meso*-C
(a) ^1H and ^{13}C NMR (CD_2Cl_2, 223 K)						
OETPP	–	−37.2	–	45.1	–	416.2
TPP	−26.1	25.2	−8.7	65.1	11.7	997.3
T^nPrP	−21.5	73.1	−3.5	336.1	12.7	[a]
T^cPrP	−18.7	97.1	4.3	386.7	14.7	[a]
T^iPrP	0.1	331.6	12.3	639.6	12.9	[a]

Porphyrins	L = Him			L = CN^-			L = ^{t}BuNC		
	g_1	g_2	g_3	g_1	g_2	g_3	g_1	g_2	g_2
(b) EPR g values (CH_2Cl_2, 4.2 K)									
OETPP	2.72	2.37	1.64	3.31	–	–	2.29	2.25	1.92
TPP	2.87	2.29	1.56	3.70	–	–	2.18	2.18	1.93
T^nPrP	2.90	2.35	1.45	2.49	2.49	–	2.16	2.16	1.96
T^cPrP	2.87	2.42	–	2.47	2.47	–	2.16	2.16	1.95
T^iPrP	2.55	2.55	–	2.42	2.42	1.74	2.16	2.16	1.95

Adapted from Refs. [25,36].
[a] Not observed.

ascending order of the pyrrole-H chemical shifts, though there is some small reversal in the order in the case of bis(^{t}BuNC) complexes. Table 4b shows the EPR g values taken in frozen CH_2Cl_2 solutions at 4.2 K, where the porphyrins are arranged in the same order as in Table 4a.

The six-coordinate iron(III) porphyrinates listed in Table 4 have various structures such as saddled, planar, and ruffled structures as shown in Fig. 7; OETPP shown in Scheme 1g has saddled structure, TPP shown in Scheme 1b where X = H usually exhibits planar structure, and TRP's such as T^{n}PrP, T^{c}PrP, and T^{i}PrP shown in Scheme 1c have ruffled structure [46–52]. It should be noted that the structures of $[Fe(TPP)L_2]^{\pm}$ easily change depending on the nature of axial ligands. For example, both $[Fe(TPP)(^t BuNC)_2]^+$ and $[Fe(TMP)(1,2\text{-}Me_2Im)_2]^+$ have highly ruffled porphyrin cores despite the presence of usually planar TPP and TMP [6,16,53]. As mentioned, the former complex ruffles due to the bonding interaction between d_{xy} and a_{2u} orbitals while the latter ruffles due to the severe steric repulsion between porphyrin core and bulky 1,2-Me_2Im.

In the case of bis(Him) complexes, EPR data suggest that all the complexes except $[Fe(T^iPrP)(HIm)_2]^+$ adopts the $(d_{xy})^2(d_{xz},d_{yz})^3$ ground state; only the T^{i}PrP complex shows the $(d_{xz},d_{yz})^4(d_{xy})^1$ ground state at 4.2 K [25]. This is actually the only example that bis(HIm) complex adopts the less common $(d_{xz},d_{yz})^4(d_{xy})^1$ ground state, which will be further discussed later. Corresponding to the EPR results, the NMR results taken at much higher temperature also support this conclusion. The pyrrole-H signal of $[Fe(T^iPrP)(HIm)_2]^+$ appears at +0.1 ppm at 223 K, which is at least by 19 ppm much more downfield than the corresponding signals of other complexes. Similarly, the *meso*-C signal of $[Fe(T^iPrP)(HIm)_2]^+$ is observed at 332 ppm at 223 K, which is at least by 230 ppm much more downfield than the corresponding signals of the other complexes. As mentioned, the presence of the downfield shifted pyrrole-H and *meso*-C signals are the characteristic features of low-spin complexes adopting the $(d_{xz},d_{yz})^4(d_{xy})^1$ ground state. Since the electronic effects of alkyl substituents such as propyl, cyclopropyl and isopropyl groups are considered to be similar, the difference in electronic ground states among $[Fe(T^nPrP)(HIm)_2]^+$, $[Fe(T^cPrP)(HIm)_2]^+$, and $[Fe(T^iPrP)(HIm)_2]^+$ can best be explained in terms of the difference in the degree of ruffling. That is, the d_{xy} orbital in $[Fe(T^iPrP)(HIm)_2]^+$ interacts most effectively with the a_{2u} orbital since the porphyrin ring of this complex is most strongly ruffled. Thus, we can say that the $(d_{xz},d_{yz})^4(d_{xy})^1$ ground state can be stabilized as the degree of ruffling of the porphyrin ring increases.

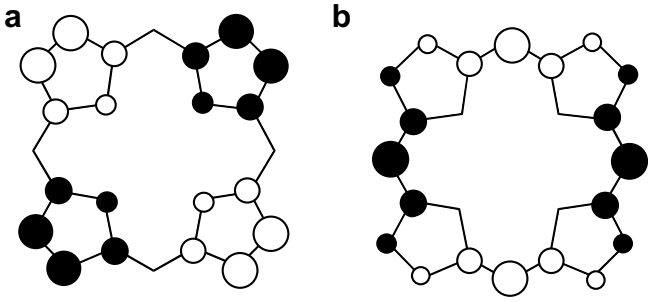

Fig. 7. Major deformation modes of porphyrin: (a) saddle and (b) ruffle. Open circles represent atoms above the least-squares plane, and the filled circles correspond to atoms below the plane.

There are several more examples suggesting that the ruffled deformation stabilizes the $(d_{xz},d_{yz})^4(d_{xy})^1$ ground state. As shown in Table 1, the pyrrole-H signal in $[Fe(TMP)(2\text{-}MeIm)_2]^+$ appears at −20.4 ppm which is by 11 ppm more downfield than that in $[Fe(TMP)(1\text{-}MeIm)_2]^+$. Similarly, the data in Table 2 indicate that the pyrrole-H signal in $[Fe(T^nPrP)(2\text{-}MeIm)_2]^+$ appears at −8.2 ppm which is by 13 ppm more downfield than that in $[Fe(T^nPrP)(HIm)_2]^+$. Furthermore, the pyrrole-H signals in a series of $[Fe(TRP)(2\text{-}MeIm)_2]^+$ appear at −21.7, −8.2, −9.4, +5.7 ppm at 238 K for the R = H, Me, Et, and ^{i}Pr complexes, respectively [54]. The result can be explained in terms of a smooth change of electronic ground state from $(d_{xy})^2(d_{xz},d_{yz})^3$ to $(d_{xz},d_{yz})^4(d_{xy})^1$ caused by the ruffling of the porphyrin core [36]. The difference in chemical shifts of the *meso*-C signals in a series of $[Fe(TMP)L_2]^+$ can be explained similarly; they are 40 ppm (L = 1-MeIm), 80 and 150 ppm (L = 2-MeIm), 128 ppm (L = BzIm), and 321 ppm (L = 2-MeBzIm) at 221 K [55,56]; the *meso*-C signal splits into two signals in $[Fe(TMP)(2\text{-}MeIm)_2]^+$ due to the slow rotation of the coordinated 2-MeIm ligands around the Fe–N bond on the NMR timescale. Granted that the field strengths of these imidazole ligands are different, the major reason for the downfield shifts of the pyrrole-H and *meso*-C signals on going from the less bulky to bulky imidazole ligands should be ascribed to the change in electronic ground state from $(d_{xy})^2(d_{xz},d_{yz})^3$ to $(d_{xz},d_{yz})^4(d_{xy})^1$, which is caused by the ruffling of the porphyrin core due to the steric repulsion between the axial ligands and the porphyrin core. In Fig. 8 are given two such examples, $[Fe(TMP)(1,2\text{-}Me_2Im)_2]^+$ and $[Fe(TEtP)(2\text{-}MeIm)_2]^+$, where the severe steric repulsion between bulky axial ligands and porphyrin core extremely ruffles the porphyrin ring [53,57].

In the case of bis(CN^-) complexes, both NMR and EPR data suggest that the OETPP and TPP complexes adopt the $(d_{xy})^2(d_{xz},d_{yz})^3$ ground state while other three complexes of *meso*-tetraalkylporphyrins(TRP's) adopt the $(d_{xz},d_{yz})^4(d_{xy})^1$ ground state [25]. Latos-Grazynski, Marchon and co-workers also reported the complexes with the less common $(d_{xz},d_{yz})^4(d_{xy})^1$ ground state in alkyl substituted porphyrins [40,42].

In the case of bis(^{t}BuNC) complexes, all the complexes listed in Table 4 show the $(d_{xz},d_{yz})^4(d_{xy})^1$ ground state. Close inspection of the EPR data of these complexes reveals, however, that the energy gap between the d_{xy} and d_π orbitals increases in the order, OETPP < TPP < T^{n}PrP, T^{c}PrP, T^{i}PrP. However, it is difficult to say if this order indicates that the saddled deformation of the porphyrin ring stabilizes the $(d_{xy})^2(d_{xz},d_{yz})^3$ ground state. This is

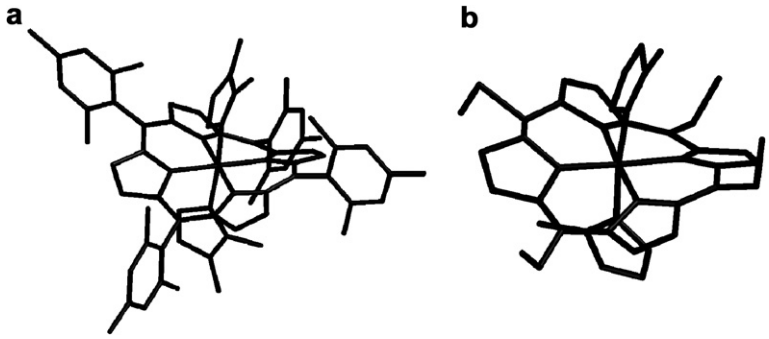

Fig. 8. ORTEP diagrams of (a) $[Fe(TMP)(1,2\text{-}Me_2Im)_2]^+$ and (b) $[Fe(TEtP)(2\text{-}MeIm)_2]^+$. Adapted from Refs. [53,57].

because OETPP has eight ethyl groups at the pyrrole β positions as compared with TPP, which should affect the electronic ground state of low-spin iron(III) complexes. We consider, however, that the saddled deformation could stabilize the $(d_{xy})^2(d_{xz},d_{yz})^3$ ground state since the d_π orbitals are destabilized by the d_π–$3e_g$ interactions which is expected to be much stronger in saddled OETPP complexes than in planar TPP complexes due to the effective orbital overlaps. On the basis of these results, we have concluded that the $(d_{xz},d_{yz})^4(d_{xy})^1$ ground state is stabilized if the porphyrin ring ruffles, while the $(d_{xy})^2(d_{xz},d_{yz})^3$ ground state is stabilized if the porphyrin ring is saddled.

Quite recently, Yatsunyk and Walker reported that $[Fe(OMTPP)(^t BuNC)_2]^+$ has a purely saddled porphyrin core in the solid though it adopts the $(d_{xz},d_{yz})^4(d_{xy})^1$ ground state [58]. Therefore, the authors have emphasized that, although a ruffled geometry stabilizes the $(d_{xz},d_{yz})^4(d_{xy})^1$ ground state, the ruffling is not necessary for the existence of the $(d_{xz},d_{yz})^4(d_{xy})^1$ ground state. However, $[Fe(OMTPP)(^t BuNC)_2]^+$ shows the *meso*-C signal at extremely downfield position, i.e. 979 ppm at 223 K, which is quite close to that of $[Fe(TPP)(^t BuNC)_2]^+$, 997 ppm [25]. The result clearly indicates that the *meso*-carbons of $[Fe(OMTPP)(^t BuNC)_2]^+$ certainly have large amounts of spin density though the complex shows purely saddled structure in the solid. The ring conformation in solution could be different from that in the solid, i.e. the highly saddled porphyrin core in $[Fe(OMTPP)(^t BuNC)_2]^+$ could include some ruffled deformation in solution. There could be an effective spin delocalization mechanism from the porphyrin to the low-spin iron(III) with the $(d_{xz},d_{yz})^4(d_{xy})^1$ electron configuration even in purely saddled $[Fe(OMTPP)(^t BuNC)_2]^+$. Obviously, both experimental and theoretical studies are necessary to reveal the spin delocalization mechanism to the *meso*-carbons in purely saddled $[Fe(OMTPP)(^t BuNC)_2]^+$ with the $(d_{xz},d_{yz})^4(d_{xy})^1$ ground state.

4. Formation of low-spin complexes with unusual electronic structures

In the previous section, the factors that affect the electronic ground state of low-spin iron(III) porphyrinates have been described in detail. By manipulating these factors, we can now prepare various low-spin complexes with unusual electronic structures. Two challenging problems that should be solved are the preparation and characterization of (i) bis(HIm) complexes with the $(d_{xz},d_{yz})^4(d_{xy})^1$ ground state and (ii) bis(^{t}BuNC) complexes with the $(d_{xy})^2(d_{xz},d_{yz})^3$ ground state. Because of the strong σ- and π-donating ability of HIm, bis(HIm) complexes adopt the $(d_{xy})^2(d_{xz},d_{yz})^3$ ground state. In contrast, because of the weak σ-donating and strong π-accepting ability of ^{t}BuNC, bis(^{t}BuNC) complexes adopt the $(d_{xz},d_{yz})^4(d_{xy})^1$ ground state. Preparation of the bis(HIm) and bis(^{t}BuNC) complexes with unusual electronic ground state, i.e. $(d_{xz},d_{yz})^4(d_{xy})^1$ and $(d_{xy})^2(d_{xz},d_{yz})^3$, respectively, and characterization of their physicochemical properties should widen our understanding on the electronic structures of iron(III) porphyrinates as well as heme proteins.

4.1. Bis(imidazole) complex adopting the $(d_{xz},d_{yz})^4(d_{xy})^1$ ground state

There is only one example of bis(HIm) complex that shows the $(d_{xz},d_{yz})^4(d_{xy})^1$ ground state [25]. The complex in question is $[Fe(T^iPrP)(HIm)_2]^+$ which satisfies the following spectroscopic conditions required for the complexes with the $(d_{xz},d_{yz})^4(d_{xy})^1$ ground state. They are (i) EPR spectrum is axial with the $g_\perp$ value to be 2.55 in frozen CH_2Cl_2 solution at 4.2 K, (ii) ^{1}H NMR spectrum shows no upfield shifted pyrrole-H signal, and (iii) ^{13}C NMR spectrum exhibits downfield shifted *meso*-C signal. The chemical shifts of the pyrrole-H and *meso*-C signals are +0.1 and 332 ppm in CD_2Cl_2 solution at 223 K. The major reason for this complex to adopt the $(d_{xz},d_{yz})^4(d_{xy})^1$ ground state should be ascribed to the presence of highly ruffled porphyrin ring together with the electron donating ability of the *meso*-isopropyl groups. How can we obtain the low-spin bis(HIm) complex with much purer $(d_{xz},d_{yz})^4(d_{xy})^1$ ground state, where the d_{xy} orbital is located far above the d_π orbitals? There is no doubt that $[Fe(T^tBuP)(HIm)_2]^+$ should give a very pure $(d_{xz},d_{yz})^4(d_{xy})^1$ type low-spin complex, since the presence of bulky *tert*-butyl groups at the *meso* positions should ruffle the prophryin ring to the greatest extent. Unfortunately, insertion of iron into T^tBuP has been

unsuccessful probably because of the narrow N4 cavity expected to this highly ruffled porphyrin ring together with the instability of the Fe^{III} complex. However, there are couple of examples of the T^{t}BuP complexes having paramagnetic metal ions such as [Cu(T^{t}BuP)] and [Mn(T^{t}BuP)(OAc)] [49,59].

4.2. Bis(tert-butylisocyanide) complex adopting the $(d_{xy})^2(d_{xz}, d_{yz})^3$ ground state

The first example of bis(^{t}BuNC) complex adopting the $(d_{xy})^2(d_{xz}, d_{yz})^3$ ground state was reported quite recently. The complex in question is not porphyrinate but diazaporphyrinate, $[Fe(DAzP)(^tBuNC)_2]^+$, shown in Scheme 1e [60]. This complex exhibits various unusual spectroscopic characteristics that have never been observed in other bis(^{t}BuNC) complexes such as $[Fe(OEP)(^tBuNC)_2]^+$ shown in Scheme 1f. The Curie plots of the α-CH_2 and *meso*-H signals given in Fig. 9 clearly show the difference in electronic structures between $[Fe(DAzP)(^tBuNC)_2]^+$ and $[Fe(OEP)\ (^tBuNC)_2]^+$. The differences in spectroscopic properties are as follows: (i) The α-CH_2 signals of $[Fe(DAzP)(^tBuNC)_2]^+$ and $[Fe(OEP)(^tBuNC)_2]^+$ are observed at $\delta = 17.8$ and 7.6 ppm at 298 K, respectively, suggesting that $[Fe(DAzP)(^tBuNC)_2]^+$ has sizable amount of spin density at the pyrrole β carbons. (ii) The *meso*-H signals of $[Fe(DAzP)(^tBuNC)_2]^+$ and $[Fe(OEP)(^tBuNC)_2]^+$ appear at $\delta = 19.2$ and -37.7 ppm, respectively, indicating that the *meso*-C's of $[Fe(DAzP)(^tBuNC)_2]^+$ have a negative spin, -0.012, while those of $[Fe(OEP)(^tBuNC)_2]^+$ have a large positive spin, $+0.028$. (iii) While the *meso*-C signal of $[Fe(DAzP)(^tBuNC)_2]^+$ appears at 21 ppm at 223 K, that of $[Fe(OEP)(^tBuNC)_2]^+$ appears at 491 ppm. (iv) EPR spectrum of $[Fe(DAzP)(^tBuNC)_2]^+$ shown in Fig. 10 is rhombic as in the case of $[Fe(DAzP)(DMAP)_2]^+$. These results strongly indicate that $[Fe(DAzP)(^tBuNC)_2]^+$ adopts the $(d_{xy})^2(d_{xz}, d_{yz})^3$ ground state despite the coordination of ^{t}BuNC. The IR spectroscopic data given below is instructive. The CN stretching frequency of the coordinating ^{t}BuNC in $[Fe(DAzP)(^tBuNC)_2]^+$ is 2213 cm^{-1}, which is by 13–20 cm^{-1} higher than the corresponding values of all the other bis(^{t}BuNC) complexes. The higher frequency indicates the stronger σ-bonding and/or the weaker π-back bonding in $[Fe(DAzP)(^tBuNC)_2]^+$ as compared with those in other bis(^{t}BuNC) complexes. A reasonable explanation is that, because of the presence of two electronegative nitrogen atoms at the *meso* positions, the a_{2u} type orbital in DAzP is stabilized as shown in Fig. 6b and that the a_{2u}–d_{xy} interaction is therefore weakened. The weak a_{2u}–d_{xy} interaction, which indicates the weak porphyrin to iron(III) charge transfer, makes the iron(III) ion electron poor. Consequently, the σ-donation from ^{t}BuNC is strengthened and/or π-back donation from iron(III) is weakened, both of which contribute to the higher CN stretching in $[Fe(DAzP)(^tBuNC)_2]^+$ as compared with other bis(^{t}BuNC) complexes.

More recently, bis(^{t}BuNC) complex that adopts the $(d_{xy})^2(d_{xz}, d_{yz})^3$ ground state has been found even in porphyrinate [61]. The complex in question is [Fe(OETArP)(^{t}BuNC)$_2$]$^+$ shown in Scheme 1h, where Ar is 3,5-bis(trifluoromethyl)phenyl and L = ^{t}BuNC. This complex gives a rhombic type EPR spectrum with $g = 2.524$, 2.186, and 1.859. Correspondingly, the ^{13}C NMR spectrum exhibits no downfield shifted *meso*-C signal; the *meso*-C signal is observed at 161 ppm at 298 K. The spectroscopic data of $[Fe(OETArP)(^tBuNC)_2]^+$ are quite different from those of analogous $[Fe(OETAr'P)(^tBuNC)_2]^+$ shown in Scheme 1i, where Ar′ = 4-methoxlyphenyl and L = ^{t}BuNC. The EPR spectrum of $[Fe(OETAr'P)(^tBuNC)_2]^+$ is axial with $g_\perp = 2.216$ and $g_\parallel = 1.925$. The ^{13}C NMR spectrum shows downfield shifted *meso*-C signal at 430 ppm. Thus, it is quite reasonable that the complex shown in Scheme 1(h) adopts the $(d_{xy})^2(d_{xz}, d_{yz})^3$ ground state despite the coordination of ^{t}BuNC while the complex shown in Scheme 1i adopts the $(d_{xz}, d_{yz})^4(d_{xy})^1$ ground state. Although the molecular structure of $[Fe(OETArP)(^tBuNC)_2]^+$ is not determined, the complex is supposed to have a highly saddled structure. Therefore, the unusual electronic structure should be ascribed to the highly saddled structure together with the presence of electron withdrawing *meso*-substituents.

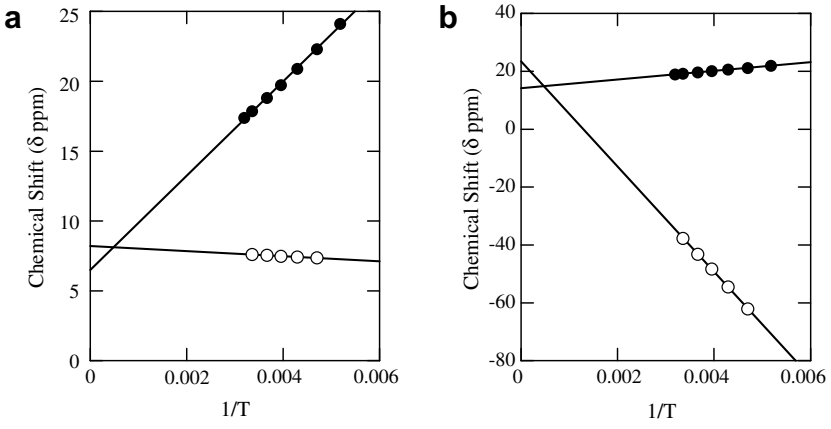

Fig. 9. Curie plots of (a) α-CH_2 and (b) *meso*-H signals. Signals in $[Fe(DAzP)(^tBuNC)_2]^+$ and $[Fe(OEP)(^tBuNC)_2]^+$ are given by • and ○, respectively. Adapted from Ref. [60].

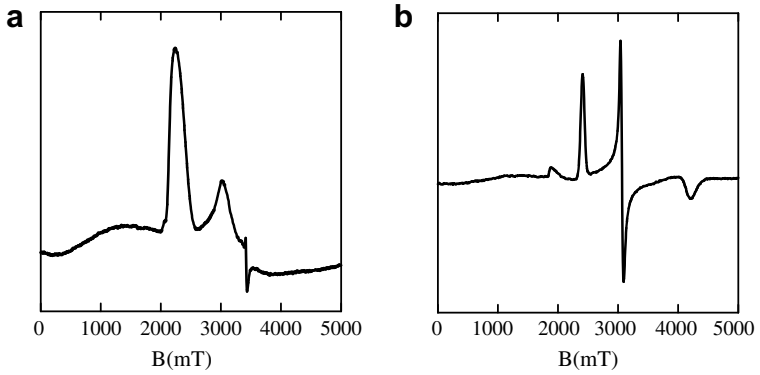

Fig. 10. EPR spectra of $[Fe(DAzP)L_2]^+$ taken in CH_2Cl_2 solutions at 4–12 K. (a) L = ^{t}BuNC and (b) L = DMAP. Adapted from Ref. [60].

5. Conclusions

Low-spin iron(III) porphyrin complexes with the common $(d_{xy})^2(d_{xz}, d_{yz})^3$ ground state show either the large g_{max}or rhombic type EPR spectra. These complexes exhibit the upfield shifted *meso*-C and pyrrole-H signals. In contrast, low-spin complexes with the less common $(d_{xz}, d_{yz})^4(d_{xy})^1$ ground state exhibit the axial type EPR spectra. In these complexes, the *meso*-C signals appear fairly downfield while the pyrrole-H signals appear quite close to their diamagnetic positions. On the basis of the EPR and NMR data, the following three factors that affect the electronic ground state have been extracted. (1) The axial ligands with weak σ donating and strong π accepting ability such as ^{t}BuNC and 4-CNPy stabilize the $(d_{xz}, d_{yz})^4(d_{xy})^1$ ground state while those with strong σ and π donating ability such as HIm and DMAP stabilize the $(d_{xy})^2(d_{xz}, d_{yz})^1$ ground state. The $(d_{xz}, d_{yz})^4(d_{xy})^1$ character increases as the axial ligand changes from HIm to ^{t}BuNC as listed below:

$$\text{HIm, 1-MeIm, DMAP} < CN^- < \text{Py} < \text{3-CNPy, 4-CNPy} < {}^t\text{BuNC}.$$

(2) Electron donating groups at the *meso*-carbons stabilize the $(d_{xz}, d_{yz})^4(d_{xy})^1$ ground state while electron withdrawing groups stabilize the $(d_{xy})^2(d_{xz}, d_{yz})^3$ ground state. Thus, the $(d_{xz}, d_{yz})^4(d_{xy})^1$ character in $[Fe(T(p\text{-X})PP)(CN)_2]^-$ increases as the Hammett σ_p value of the *p*-X substituent decreases. (3) Ruffled deformation stabilizes the $(d_{xz}, d_{yz})^4(d_{xy})^1$ ground state while the saddled deformation stabilizes the $(d_{xy})^2(d_{xz}, d_{yz})^3$ ground state. Thus, the energy gap between the d_{xy} and d_π orbitals increases in $[Fe(Porphyrin)L_2]^{\pm}$ as the porphyrin changes from saddled OETPP to planar TPP, and then to ruffled T^{i}PrP. (4) By manipulating the factors that affect the electronic ground state of low-spin iron(III) porphyrin complexes, one can obtain the complexes with unusual electronic structures such as bis(HIm) complex adopting the $(d_{xz}, d_{yz})^4(d_{xy})^1$ ground state or bis(^{t}BuNC) complex adopting the $(d_{xy})^2(d_{xz}, d_{yz})^3$ ground state; bis(HIm) and bis(^{t}BuNC) complexes always exhibit the $(d_{xy})^2(d_{xz}, d_{yz})^3$ and $(d_{xz}, d_{yz})^4(d_{xy})^1$ ground state, respectively.

6. Abbreviations

TPP 5,10,15,20-tetraphenylporphyrin
OEP 2,3,7,8,12,13,16,17-octaethyl-porphyrin
F_{20}-TPP 5,10,15,20-tetrakis(pentafluorophenyl)porphyrin
TMP 5,10,15,20-tetramesitylpoprhyrin
TRP 5,10,15,20-tetraalkylporphyrin
T(C_3F_7)P 5,10,15,20-tetrakis(heptafluoropropyl)porphyrin
TEtP 5,10,15,20-tetraethylporphyrin
T^{n}PrP 5,10,15,20-tetrapropylporphyrin
T^{c}PrP 5,10,15,20-tetracyclopropylporphyrin
T^{i}PrP 5,10,15,20-tetraisopropylporphyrin
T^{t}BuP 5,10,15,20-tetra(*tert*-butyl)porphyrin
DAzP 2,7,12,18-tetrabutyl-3,7,13,17-tetramethyl-5,15-diazaporphyrin
OMTPP 2,3,7,8,12,13,17,18-octamethyl-5,10,15,20-tetraphenylporphyrin
OETPP 2,3,7,8,12,13,17,18-octaethyl-5,10,15,20-tetraphenylporphyrin
OETArP 2,3,7,8,12,13,17,18-octaethyl-5,10,15,20-tetraarylporphyrin
TPC 5,10,15,20-tetraphenylchlorin
T(*p*-X)PP 5,10,15,20-tetrakis(*p*-substituted phenyl)porphyrin
HIm imidazole
1-MeIm 1-methylimidazole
2-MeIm 2-methylimidazole
1,2-Me_2Im 1,2-dimethylimidazole
BzIm benzimidazole
2-MeBzIm 2-methylbenzimidazole
3,4-Me_2Py 3,4-dimethylpyridine
3,5-Me_2Py 3,5-dimethylpyridine
4-MePy 4-methylpyridine
3-MePy 3-methylpyridine
Py pyridine
3-ClPy 3-chloropyridine
2-MeBzIm 2-methylbenzimidazole
DMAP 4-(*N*,*N*-dimethylamino)pyridine
3-CNPy 3-cyanopyridine
4-CNPy 4-cyanopyridine
^{t}BuNC *tert*-butylisocyanide

Acknowledgements

This work has been supported by the Research Funds for Collaborative Project in Toho University (2007), by the Research Center for Materials with Integrated Properties (High-Tech Research Center), Toho University, and by the Grant in Aid for Scientific Research from Ministry of Education, Culture, Sports, Science and Technology, Japan. The authors thank Professors Saburo Neya of Chiba University and Masashi Takahashi of Toho University for helpful discussions. The authors also thank his current and former graduate students who have significantly contributed to the work reported from this laboratory that is referenced in this review: Takahisa Ikeue, Yumiko Kawasaki, Takashi Saitoh, Mari Fukagawa, Takanori Sakai, Nao Takahashi, Akito Hoshino, Yuya Chiba, and Hajime Eguchi.

References

[1] W. Kaim, B. Schwederski, Bioinorganic Chemistry: Inorganic Elements in the Chemistry of Life, John Wiley & Sons Inc., New York, 1994.
[2] P.R. Ortiz de Montellano, Cytochrome P450: Structure, Mechanism, and Biochemistry, second ed., Plenum, New York, 1995.
[3] K. Auclair, Z. Hu, D.M. Little, P.R. Ortiz de Montellano, J.T. Groves, J. Am. Chem. Soc. 124 (2002) 6020–6027.
[4] E.I. Solomon, A.B.P. Lever (Eds.), Inorganic Electronic Structure Spectroscopy, vol. 1, John Wiley & Sons Inc., New York, 1999.
[5] L. QueJr. (Ed.), Physical Method in Bioinorganic Chemistry, University Science Books, Sausalito, CA, 2000.
[6] W.R. Scheidt, in: K.M. Kadish, K.M. Smith, R. Guilard (Eds.), The Porphyrin Handbook, vol. 3, Academic Press, San Diego, CA, 2000, pp. 49–112, ch. 16.
[7] M. Nakamura, Coord. Chem. Rev. 250 (2006) 2271–2294.
[8] F.A. Walker, in: K.M. Kadish, K.M. Smith, R. Guilard (Eds.), The Porphyrin Handbook, vol. 5, Academic Press, San Diego, 2000, pp. 81–183 (Chapter 36).
[9] F.A. Walker, Inorg. Chem. 42 (2003) 4526–4544.
[10] F.A. Walker, Chem. Rev. 104 (2004) 589–616.
[11] M.K. Safo, G.P. Gupta, C.T. Watson, U. Simonis, F.A. Walker, W.R. Scheidt, J. Am. Chem. Soc. 114 (1992) 7066–7075.
[12] M.K. Safo, F.A. Walker, A.M. Raitsimring, W.P. Walters, D.P. Dolata, P.G. Debrunner, W.R. Scheidt, J. Am. Chem. Soc. 116 (1994) 7760–7770.
[13] M.R. Cheesman, F.A. Walker, J. Am. Chem. Soc. 118 (1996) 7373–7380.
[14] R.-J. Cheng, P.-Y. Chen, T. Lovell, Liu T, L. Noodleman, D.A. Case, J. Am. Chem. Soc. 125 (2003) 6774–6783.
[15] J. Cjonradie, A. Ghosh, J. Phys. Chem. B 107 (2003) 6486–6490.
[16] F.A. Walker, H. Nasri, I. Turowska-Tyrk, K. Mohanrao, C.T. Watson, N.V. Shokhirev, P.G. Debrunner, W.R. Scheidt, J. Am. Chem. Soc. 118 (1996) 12109–12118.
[17] M.-A. Pilard, M. Guillemot, L. Toupet, J. Jordanov, G. Simonneaux, Inorg. Chem. 36 (1997) 6307–6314.
[18] G. Simonneaux, V. Schünemann, C. Morice, L. Carel, L. Toupet, H. Winkler, A.X. Trautwein, F.A. Walker, J. Am. Chem. Soc. 122 (2000) 4366–4377.
[19] G.N. La Mar, F.A. Walker, in: D. Dolphin (Ed.), The Porphyrin, vol. 4, Academic Press, New York, 1979, pp. 57–161 (Chapter 2).
[20] H.M. Goff, in: A.B.P. Lever, H.B. Gray (Eds.), Physical Bioinorganic Chemistry Series 1, Iron Porphyrin I, Nuclear Magnetic Resonance of Iron Porphyrins, Addison-Wesley, Reading, MA, 1983, pp. 237–281.
[21] F.A. Walker, U. Simonis, in: L.J. Berliner, J. Reuben (Eds.), NMR of Paramagnetic Molecules, vol. 12, Plenum Press, New York, 1993, pp. 133–274.
[22] I. Bertini, C. Luchinat, in: A.B.P. Lever (Ed.), NMR of Paramagnetic Substances, Coord. Chem. Rev, vol. 150, Elsevier, Amsterdam, 1996, pp. 29–75.
[23] M. Rivera, G.A. Caignan, Anal. Bioanal. Chem. 378 (2004) 1464–1483.
[24] J.D. Satterlee, G.N. La Mar, J. Am. Chem. Soc. 98 (1976) 2804–2808.
[25] T. Ikeue, Y. Ohgo, T. Saitoh, T. Yamaguchi, M. Nakamura, Inorg. Chem. 40 (2001) 3423–3434.
[26] G. Simonneaux, F. Hindre, M. Le Plouzennec, Inorg. Chem. 28 (1989) 823–825.
[27] C. Geze, N. Legrand, A. Bondon, G. Simonneaux, Inorg. Chim. Acta 195 (1992) 73–76.
[28] G. Palmer, in: A.B.P. Lever, H.B. Gray (Eds.), Iron Porphyrins, Part II, Physical Bioinorganic Chemistry Series, vol. 2, Addison-Wesley, Reading, MA, 1983, pp. 43–88.
[29] A. Bencini, D. Gatteschi, in: E.I. Solomon, A.B.P. Lever (Eds.), Inorganic Electronic Structure Spectroscopy, vol. 1, John Wiley & Sons Inc., New York, 1999, pp. 131–159.
[30] T. Ikeue, T. Yamaguchi, Y. Ohgo, M. Nakamura, Chem. Lett. (2000) 342–343.
[31] C.P.S. Taylor, Biochim. Biophys. Acta 491 (1977) 137–149.
[32] T.L. Bohan, J. Magn. Reson. 26 (1977) 109–118.
[33] M. Guillemot, G. Simonneaux, J. Chem. Soc. Chem. Commun. (1995) 2093–2094.
[34] G. Simonneaux, P. Sodano, Inorg. Chem. 27 (1988) 3956–3959.
[35] M.M. Rahman, H.Y. Liu, K. Ericks, A. Prock, W.P. Giering, Organometallics 8 (1989) 1–7.
[36] T. Ikeue, Y. Ohgo, T. Saitoh, M. Nakamura, H. Fujii, M. Yokoyama, J. Am. Chem. Soc. 122 (2000) 4068–4076.
[37] A. Ikezaki, T. Ikeue, M. Nakamura, Inorg. Chim. Acta 335 (2002) 91–99.
[38] G.N. La Mar, J.D. Gaudio, J.S. Frye, Biochim. Biophys. Acta 498 (1977) 422–435.
[39] M. Nakamura, T. Ikeue, H. Fujii, T. Yoshimura, J. Am. Chem. Soc. 119 (1997) 6284–6291.
[40] S. Wolowiec, L. Latos-Grazynski, M. Mazzanti, J.-C. Marchon, Inorg. Chem. 36 (1997) 5761–5771.
[41] J. Wojaczynski, L. Latos-Grazynski, T. Glowiak, Inorg. Chem. 36 (1997) 6299–6306.
[42] S. Wolowiec, L. Latos-Grazynski, D. Toronto, J.-C. Marchon, Inorg. Chem. 37 (1998) 724–732.
[43] M. Nakamura, T. Ikeue, H. Fujii, T. Yoshimura, K. Tajima, Inorg. Chem. 37 (1998) 2405–2414.
[44] M. Nakamura, T. Ikeue, A. Ikezaski, Y. Ohgo, H. Fujii, Inorg. Chem. 38 (1999) 3857–3862.
[45] K.T. Moore, J.T. Fletcher, M.J. Therien, J. Am. Chem. Soc. 121 (1999) 5196.
[46] W. Jentzen, M.C. Simpson, J.D. Hobbs, X. Song, T. Ema, N.Y. Nelson, C.J. Medforth, K.M. Smith, M. Veyrat, M. Mazzanti, R. Ramasseul, J.-C. Marchon, T. Takeuchi, E.A. Goddard III, J.A. Shelnutt, J. Am. Chem. Soc. 117 (1995) 11085–11097.
[47] M.O. Senge, T. Ema, K.M. Smith, J. Chem. Soc. Chem. Commun. (1995) 733–734.
[48] M. Veyrat, R. Ramasseul, J.-C. Marchon, I. Turowska-Tyrk, W.R. Schiedt, New J. Chem. 19 (1995) 1199–1202.
[49] M.O. Senge, I. Bischoff, N.Y. Nelson, K.M. Smith, J. Porphyr. Phthalocya. 3 (1999) 99–116.
[50] K.M. Barkigia, L. Chantranupong, K.M. Smith, J. Fajer, J. Am. Chem. Soc. 110 (1988) 7566–7567.
[51] K.M. Barkigia, M.D. Berber, J. Fajer, C.J. Medforth, M.W. Renner, K.M. Smith, J. Am. Chem. Soc. 112 (1990) 8851–8857.
[52] C.J. Medforth, M.O. Senge, K.M. Smith, L.D. Sparks, J.A. Shelnutt, J. Am. Chem. Soc. 114 (1992) 9859–9869.
[53] O.Q. Munro, H.M. Marques, P.G. Debrunner, K. Mohanrao, W.R. Scheidt, J. Am. Chem. Soc. 117 (1995) 935–954.

[54] M. Nakamura, T. Ikeue, S. Neya, N. Funasaki, N. Nakamura, Inorg. Chem. 35 (1996) 3731–3732.
[55] M. Nakamura, K. Tajima, K. Tada, K. Ishizu, N. Nakamura, Inorg. Chem. Acta 224 (1994) 113–124.
[56] M. Nakamura, N. Nakamura, Chem. Lett. (1991) 1885–1888.
[57] Y. Ohgo, T. Ikeue, T. Saitoh, M. Nakamura, Chem. Lett. (2002) 42–43.
[58] L.A. Yatsunyk, F.A. Walker, Inorg. Chem. 43 (2004) 4341–4352.
[59] A. Ikezaki, M. Nakamura, Chem. Lett. 34 (2005) 1046–1047.
[60] Y. Ohgo, S. Neya, H. Uekusa, M. Nakamura, Chem. Commun. (2006) 4590–4592.
[61] Y. Ohgo, A. Hoshino, T. Okamoto, H. Uekusa, D. Hashizume, A. Ikezaki, M. Nakamura, Inorg. Chem. 46 (2007) 8193–8207.